Synthetic Three-Dimensional $\mathbb{Z} \times \mathbb{Z}_2$ Topological Insulator in an Elastic Metacrystal

Wei Wang, Ze-Guo Chen, and Guancong Ma*
Department of Physics, Hong Kong Baptist University, Kowloon Tong, Hong Kong, China

(Received 20 April 2021; revised 21 July 2021; accepted 12 October 2021; published 17 November 2021)

We report a three-dimensional (3D) topological insulator (TI) formed by stacking identical layers of Chern insulators in a hybrid real-synthetic space. By introducing staggered interlayer hopping that respects mirror symmetry, the bulk bands possess an additional $\mathbb{Z}_2$ topological invariant along the stacking dimension, which, together with the nontrivial Chern numbers, endows the system with a $\mathbb{Z} \times \mathbb{Z}_2$ topology. A 4-tuple topological index characterizes the system's bulk bands. Consequently, two distinct types of topological surface modes (TSMs) are found localized on different surfaces. Type-I TSMs are gapless and are protected by Chern numbers, whereas type-II gapped TSMs are protected by $\mathbb{Z}_2$ bulk polarization in the stacking direction. Remarkably, each type-II TSM band is also topologically nontrivial, giving rise to second-order topological hinge modes (THMs). Both types of TSMs and the THMs are experimentally observed in an elastic metacrystal.

DOI: 10.1103/PhysRevLett.127.214302

The study of band topology has led to the discovery of a kaleidoscope of topologically nontrivial systems across many realms in physics [1–6], and is the focus of many theoretical and experimental investigations. A Bloch band is a compact manifold, and its topological characterization depends on dimensionality [7–9], which can be either reciprocal or synthetic or both. For even-dimensional bands, an integer topological invariant known as Chern number can be obtained by surface integrating their Berry curvature [10,11]. For odd-dimensional systems, one can compute the Chern-Simons integral, which yields quantized values under chiral or inversion symmetry [9]. For example, the Chern-Simons integral of one-dimensional (1D) Bloch bands, such as those of a Su-Schrieffer-Heeger chain, is equivalent to the winding number of the Berry connection across the Brillouin zone, producing the well-known Zak phase [12]. Because of the connection of the Berry phase with the electrical polarization in crystalline solids [13–17], the 1D Chern-Simons integral can also be computed for the Berry connection defined along each dimension in a higher-dimensional crystal. The results then yield a bulk polarization, which can be quantized under certain symmetries, thus becoming a topological invariant. This idea has significantly enriched the topological band theory by revealing the higher-order topological insulators (TIs) [18,19].

The ascension to three dimensions (3D) has led to a richer diversity of band topology. On the one hand, 3D band topology can sometimes be characterized by a 3D Chern-Simons invariant that associates with magnetoelectric polarizability [7,9,20–22]. On the other hand, an alternative way is to consider a combination of three invariants defined on three orthogonal 2D tori T^2 obtained by slicing the 3D bands which are T^3 [9]. Following the discovery of quantum spin-Hall phase [23–25] and topological crystalline insulators [26], it was shown that 2D and 3D topological invariants are both needed to form the combination $[\nu_0, (\nu_1, \nu_2, \nu_3)]$ for the classification of the 3D "strong" and "weak" TIs [27–29]. A 3D strong TI has nonzero 3D Chern-Simons invariant (the index ν_0) [30],

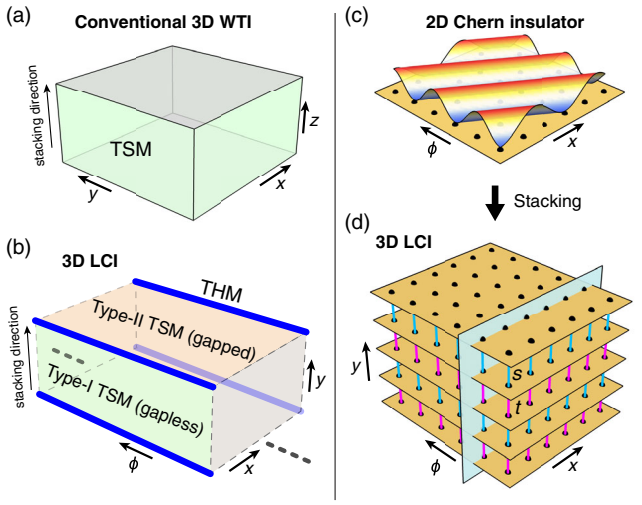

FIG. 1. (a) A conventional 3D WTI constructed by stacking 2D TIs exhibits TSMs only on surfaces parallel to the stacking direction. (b) The proposed 3D LCI sustains two types of TSMs localized on different surfaces. In addition, it sustains second-order THMs. (c) A schematic drawing of 2D Chern insulator on $x\phi$ plane with one spatial and one synthetic dimension. The undulating sheet indicates the periodic modulation on hopping enforced by ϕ. (d) Stacking the 2D Chern insulators with staggered interlayer hopping t and s leads to the 3D LCI. The cyan plane marks a specific synthetic coordinate chosen for experiments.

whereas a 3D weak TI (WTI) has $\nu_0 = 0$ but $(\nu_1, \nu_2, \nu_3) \neq \mathbf{0}$, which are three $\mathbb{Z}_2$ invariants defined for T^2. Generally, a WTI can be obtained by stacking 2D TIs [27,31,32]. Topological surface modes (TSMs) in such a structure appear on surfaces parallel to the stacking direction [Fig. 1(a)]. Under additional symmetry protection, it is also possible to have TSMs appearing on all surfaces of a WTI [33]. These states are the extension of the topological boundary modes of the 2D TIs. On the other hand, the study on the band topology is not restricted to purely reciprocal dimensions. Extra dimensionality can be added to the Bloch band's manifold by incorporating synthetic dimensions, which composes of artificially engineered internal degrees of freedom [34]. Synthetic dimensions provide versatile paths to realize effective gauges, which are desirable for complex or higher-dimensional topological systems [35–39]. For example, mixing reciprocal and synthetic dimensions enables the study of Hofstadter butterfly [40] or Weyl points [41,42] in a simple lattice with one spatial dimension.

In this work, we present with both theory and experiments a 3D topological system that belongs to a $\mathbb{Z} \times \mathbb{Z}_2$ classification. Different from existing examples of 3D TIs and higher-order TIs, the bulk topology requires a 4-tuple topological invariant consisting of three Chern numbers and one quantized bulk polarization to fully characterize. The system can be regarded as a 3D layered Chern insulator (LCI) with staggered interlayer hopping [43]. Each layer is a Chern insulator existing on a 2D reciprocal-synthetic space [39,44]. Because the staggered interlayer hopping respects mirror symmetry, the 1D Chern-Simons integral along the stacking direction is quantized, thus becoming a $\mathbb{Z}_2$ invariant as the fourth topological index. As a result, our 3D LCI not only sustains gapless TSMs on surfaces parallel to the stacking direction (denoted as type-I) but also gapped TSMs protected by the $\mathbb{Z}_2$ invariant (denoted as type-II) [Fig. 1(b)]. Remarkably, the type-II TSMs are 2D topologically nontrivial bands. The 3D LCI thus also supports (3-2)-dimensional chiral topological hinge modes (THMs) that close the type-II TSM gaps. Further, the 3D LCI is experimentally realized using a flexural-wave elastic metacrystal. The real-space descendants of both types of TSMs and the THMs are successfully observed.

We begin by considering a 1D Harper model that is periodic in the x direction [45]. The Hamiltonian reads

$$H(k_x, \phi) = \begin{bmatrix} 0 & \kappa_1(\phi) & \kappa_3(\phi)e^{-ik_x} \\ \kappa_1^*(\phi) & 0 & \kappa_2(\phi) \\ \kappa_3^*(\phi)e^{ik_x} & \kappa_2^*(\phi) & 0 \end{bmatrix}, \quad (1)$$

wherein the modulations occur on hopping terms, i.e., $\kappa_i(\phi) = \kappa_0 + \delta\kappa\cos(2\pi b i + \phi)$ with modulation frequency $b = 1/3$, unperturbed hopping amplitude κ_0, modulation strength $\delta\kappa$, and phase factor ϕ. The parameter ϕ constitutes a synthetic dimension. This Harper chain is actually a 2D system aligned on $x\phi$ plane [Fig. 1(c)]. The system has three isolated bulk bands. The periodic modulation enforced by ϕ induces a quantized Landau flux within each unit cell, leading to nonzero Chern numbers for all three bulk bands as verified by integrating the Berry curvature $F_{k_x\phi}(\boldsymbol{k}) = \partial_{k_x}A_\phi(\boldsymbol{k}) - \partial_\phi A_{k_x}(\boldsymbol{k})$ in 2D Brillouin zone. Here, $A_{k_x(\phi)}(\boldsymbol{k}) = i\langle u(\boldsymbol{k})|\partial_{k_x(\phi)}|u(\boldsymbol{k})\rangle$ is the Berry connection wherein $u(\boldsymbol{k})$ is the eigenstate at given $\boldsymbol{k}(k_x, \phi)$ The Chern numbers are found to be 1, −2, and 1, respectively. Hence, Eq. (1) describes a 2D Chern insulator residing on $k_x\phi$ plane [44,45]. When truncated in the x direction, gapless topological boundary modes protected by the nonzero Chern numbers are found, as displayed in Fig. 2(a).

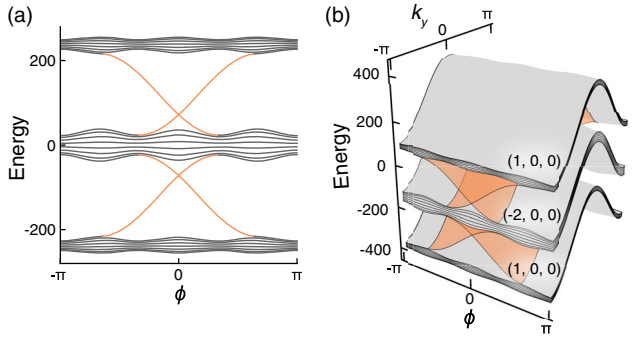

FIG. 2. (a) Eigenspectra of a finite Harper chain as a function of ϕ with parameters $\kappa_0 = 120$, $\delta\kappa = 96$. (b) Eigenspectra of the 3D system truncated in x direction with uniform interlayer hopping, i.e., $t = s$. The bulk Chern numbers $(C_{x\phi}, C_{y\phi}, C_{xy})$ are indicated in (b).

Stacking the 2D Chern insulator along the y direction leads to a 3D LCI in a hybrid real-synthetic space, as illustrated in Fig. 1(d). Here, we explore the interlayer hopping, denoted as t and s, as a new degree of freedom. We first set $t = s$. In this case, the unit cell consists of three sites and the LCI is described by a three-level Hamiltonian $\mathscr{H}_{t=s}(k_x, \phi, k_y) = H(k_x, \phi) + (2t\cos k_y)I_3$, where I_3 is a 3×3 identity. The 3D Brillouin zone is isomorphic to a T^3. The bulk band topology can be characterized by slicing the T^3 to T^2's on three orthogonal planes. An integer invariant, i.e., Chern number, can be computed for each T^2 as $C_{\mu\nu}(k_\varepsilon) = (1/2\pi)\int \mathrm{Tr}(F_{\mu\nu})dk_\mu dk_\nu$, with μ, ν, ε cyclically indexing the dimensions. Therefore, a triad of $(C_{x\phi}, C_{y\phi}, C_{xy})$ can fully describe the 3D bulk topology. We found that $C_{x\phi}$ are 1, −2, and 1 for the three bulk bands, respectively, and they are constant in k_y. Meanwhile, $C_{y\phi} = C_{xy} = 0$. We remark that these Chern numbers are computed by slicing the 3D bulk bands, instead of using a single 2D layer. Therefore, the bulk band topology of this 3D LCI falls into a $\mathbb{Z}$ classification. Bulk-surface correspondence indicates the existence of gapless TSMs on the ϕy surface, as depicted in Fig. 2(b).

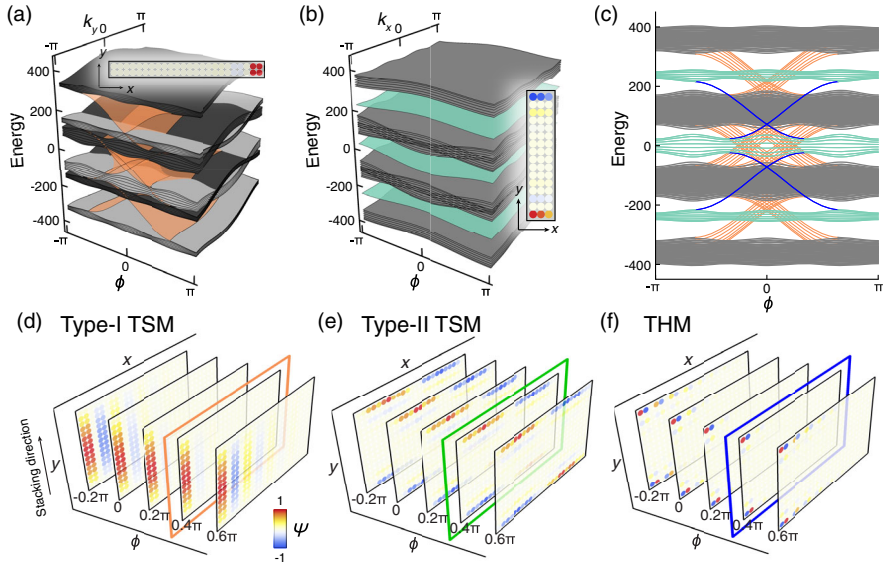

FIG. 3. (a) Eigenspectra of the 3D LCI when truncated (a) in x direction, (b) in y direction, and (c) in both x and y directions. The black and gray bands respectively belong to the two blocks $M_\pm$ in Eq. (4). Inset in (a): eigenstate of the type-I TSMs at $(\phi = 0.4\pi, k_y = -\pi)$. Inset in (b): eigenstate of the type-II TSMs at $(\phi = 0.5\pi, k_x = 0)$. Eigenstates of (d) the type-I TSMs, (e) the type-II TSMs, and (f) the THMs as a function of ϕ. The colored boxes in (d)–(f) mark $\phi = 0.4\pi$, which is the synthetic coordinate for experiment.

Next, we introduce staggered interlayer hopping, i.e., $t \neq s$. The first consequence is the doubling of the sites per unit cell, hence the Hamiltonian becomes a 6×6 matrix

$$\mathscr{H}(k_x, \phi, k_y) = \begin{bmatrix} H(k_x, \phi) & (t + se^{-ik_y})I_3 \\ (t + se^{ik_y})I_3 & H(k_x, \phi) \end{bmatrix}. \quad (2)$$

Interestingly, Eq. (2) can be block diagonalized by a similarity transformation $\tilde{\mathscr{H}} = W^{-1}\mathscr{H}W$, where

$$W = \begin{pmatrix} 1 & w \\ -w^{-1} & 1 \end{pmatrix} \otimes I_3, \quad (3)$$

and $w = -\sqrt{(t + se^{-ik_y})/(t + se^{ik_y})}$. The outcome is

$$\tilde{\mathscr{H}} = \begin{pmatrix} M_+ & 0 \\ 0 & M_- \end{pmatrix}, \quad (4)$$

wherein $M_\pm = H(k_x, \phi) \pm V(k_y)I_3$ and $V(k_y) = \sqrt{t^2 + s^2 + 2ts\cos k_y}$. Equation (4) implies that the 3D LCI is equivalent to two copies 3D TIs described by $M_\pm$. Then, we can characterize the bulk band topology of the 3D LCI by computing the Chern numbers of the bulk bands of each block. It is found that the Chern numbers $C_{x\phi}$ for the three bulk bands of each block are quantized to be 1, −2, and 1, respectively, while $C_{y\phi} = C_{xy} = 0$. Thus, each copy of 3D TIs produces its own gapless type-I TSMs, as shown in Fig. 3(a). Depending on the magnitudes of t and s, the bulk bands from these two blocks can overlap. When $t = 30$ and $s = 120$, the 3D LCI exhibits four bulk bands, in which the second and third bands are the overlap of one M_+ band and one M_- band [Fig. 3(a)].

The staggered interlayer hopping introduces additional nontrivial topology in the stacking direction. To show this, we compute the Wannier bands $w_y = (1/2\pi)\int_{-\pi}^{\pi} \mathrm{Tr}(A_{k_y})dk_y$, where $A_{k_y} = i\langle u(\boldsymbol{k})|\partial_{k_y}|u(\boldsymbol{k})\rangle$ is the Berry connection in the k_y direction. Note that w_y is equivalent to a 1D Chern-Simons integral. When $|t/s| < 1$, $w_y = 1/2$ for all bands for all (k_x, ϕ), which is the consequence of mirror symmetry. This result indicates that the 3D LCI has a quantized bulk polarization along the stacking direction $P_y = [1/(2\pi)^2]\int_\Omega w_y dk_x d\phi = \frac{1}{2}$, where Ω is the $k_x\phi$ plane of the 3D Brillouin zone. We have also confirmed that $w_y = 0$ for all bands when $|t/s| > 1$. We have further computed w_x and w_ϕ. The results are not quantized, which conforms with the absence of the mirror symmetry along x and ϕ directions. The above analyses show that our 3D LCI has a combined $\mathbb{Z} \times \mathbb{Z}_2$ bulk topology, which is fully characterized by a 4-tuple topological index $(C_{x\phi}, C_{y\phi}, C_{xy}; P_y)$. Such a topological index combination clearly sets our system apart from the 3D TIs that are characterized by combinations of $\mathbb{Z}_2$ indices.

The quantized nonzero P_y protects a different type of TSMs (type-II). In Fig. 3(b), we see three bands of the type-II TSMs (teal), which owe their existence to the nonzero P_y and they do not close the bulk band gaps. The type-II TSMs are localized on $x\phi$ planes, as shown in Fig. 3(e). Since the three type-II TSMs are 2D bands on $k_x\phi$ plane, we can further compute their Chern numbers and found $C_{x\phi}^{\mathrm{TSM}} = 1, -2, 1$, respectively. In other words, all three

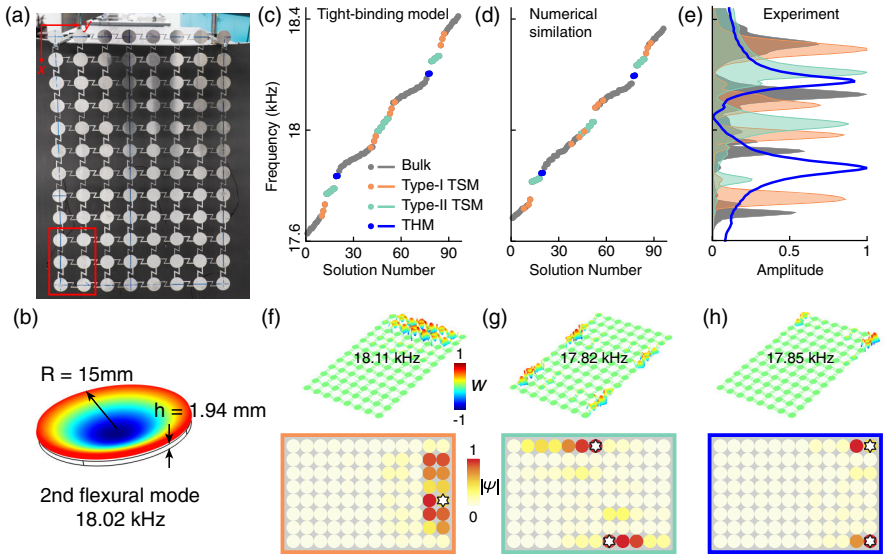

FIG. 4. (a) A photograph of the elastic metacrystal consisting of 12×8 disks. (b) The second-order flexural eigenmode (18.02 kHz) of an isolated disk. (c) Eigenfrequencies of the 3D LCI at $\phi = 0.4\pi$ calculated by the tight-binding model and (d) the finite element method. (e) The measured response spectra of the bulk modes (gray shaded region), the type-I TSMs (orange), the type-II TSMs (teal), and the THMs (blue). (f)–(h) Simulated (top) and measured (bottom) out-of-plane displacement fields of the TSMs and THMs. The stars mark the source positions. It is noted that the two sources in (g) and (h) are uncorrelated and the results are independently measured and plotted together.

type-II TSM bands are topologically nontrivial. The bulk-boundary correspondence indicates the existence of topological modes that closes the TSM gaps. These findings are verified in the eigenspectra and eigenstates. As shown in Figs. 3(c)–3(f), the type-I and type-II TSMs coexist, and additional modes that make the type-II TSMs gapless are found. These modes are (3-2)-dimensional THMs that are 1D states localized in the synthetic dimension ϕ [Fig. 3(f)]. The THMs here are thus protected by the nonzero combinations of P_y and $C^{\mathrm{TSM}}_{x\phi}$, making them distinct from the previously reported higher-order topological modes.

When the interlayer hopping becomes $|t/s| > 1$ so that $P_y = 0$, both the type-II TSMs and THMs are absent [46]. It is also noteworthy that since the THMs close the type-II TSM gaps, they spectrally overlap with the 3D bulk bands when ϕ is between $\pm 0.3\pi$, thus becoming 1D bounded states in the 3D continuum [Fig. 3(c)].

When ϕ is fixed, the 3D LCI can be experimentally realized in 2D elastic-wave systems [47–51]. Here, we propose a flexural-wave metacrystal that can reproduce a tight-binding Hamiltonian with high fidelity. The system is comprised of circular disks connected with Z-shape beams [Fig. 4(a)]. The disks' second-order mode is chosen to be the onsite orbital [Fig. 4(b)]. The Z-shape beams are introduced to realize the hopping coefficients in Eq. (2), which are conveniently tunable by adjusting only the width. A systematic discussion on the metacrystal design is presented in [46]. Here, we set $\phi = 0.4\pi$, $\kappa_0 = 120$, $\delta\kappa = 96$, $t = 30$, and $s = 120$. Finite-element simulations (COMSOL Multiphysics) produce eigenspectra with good agreement with the tight-binding model (discrepancies in eigenfrequencies are $<0.28\%$), as shown in Figs. 4(c) and 4(d). By examining the vibrational profiles, the type-I, type-II TSMs, and THMs are unambiguously identified. Three representative modes are shown in Figs. 4(f)–4(h).

The elastic metacrystal is fabricated from a stainless-steel sheet using laser cutting. A waveform generator (Keysight 33500B) sends a short pulse covering 16 to 20 kHz through a voltage amplifier (Aim-TTi WA301) to a piezoelectric buzzer (radius 4.9 mm) glued to the center of a selected disk. A laser Doppler vibrometer (Polytec VGO-200) mounted on a translation stage measures the out-of-plane displacement of all disks in the lattice. The signal is recorded using a digital oscilloscope (Keysight DSO2024A). In Fig. 4(e), the gray area is the bulk response, in which four peaks are clearly seen. To measure the TSM responses, we place the buzzer at the corresponding edge (but away from the corner) and then measure the edge response several sites away. Both type-I and type-II TSMs are clearly observed [Fig. 4(e)]. We used the translational stage to scan the vibrational profiles of the entire lattice close to the peak frequencies. The results show that the modes are strongly localized along the corresponding edges, which agrees with our prediction about the TSMs [Figs. 4(f) and 4(g)]. Likewise, the THMs are observed as corner modes, as shown in Fig. 4(h). We have also fabricated and measured an additional elastic lattice with $|t/s| > 1$, in which the type-II TSMs and THMs are absent. The results are shown in [46].

In summary, we have theoretically studied and experimentally demonstrated a new type of 3D LCI that

distinguishes from previous 3D TIs. Our results show that new topological phases can be constructed by means of product topology that compounds distinct topological classes in different dimensions. This method constitutes a new strategy to engineer a diversity of novel band topology, such as the stacking of topologically distinct layers [52], or the introduction of interlayer gauge flux. The method is also suitable for analyzing topological systems in even higher dimensions [39,53]. The TSMs and gapless THMs in our system are topologically protected by unique combinations of different classes of topological indices. In particular, the THMs are distinct from the higher-order topological modes protected by quantized polarization or multipole moments [54–58], and they closely resemble the one-way hinge transport behaviors found in the 3D quantum Hall effect [31]. We anticipate that the 3D LCI is realizable in systems with only spatial dimensions, in which Chern insulating states can be achieved by breaking the time-reversal symmetry [59–61]. In this case, it is even possible to engineer THM bands with nontrivial quantized polarization such that 0D topological modes can emerge. Nevertheless, the synthetic dimensions offer additional versatility that can merit applications, such as topological waveguiding (see [46] for an example), topological Fano devices [62–64], etc. Last, our elastic metacrystal proves to be a convenient and versatile platform for realizing complex tight-binding systems, making it an excellent venue for studying topological phenomena in solids.

This work was supported by Hong Kong Research Grants Council (GRF 12302420, 12300419, ECS 22302718, CRF C6013-18G), National Natural Science Foundation of China Excellent Young Scientist Scheme (Hong Kong & Macau) (11922416) and Youth Program (11802256), and Hong Kong Baptist University (RC-SGT2/18-19/SCI/006).

*phgcma@hkbu.edu.hk

[1] M. Z. Hasan and C. L. Kane, Colloquium: Topological insulators, Rev. Mod. Phys. **82**, 3045 (2010).
[2] A. Bansil, H. Lin, and T. Das, Colloquium: Topological band theory, Rev. Mod. Phys. **88**, 021004 (2016).
[3] L. Lu, J. D. Joannopoulos, and M. Soljačić, Topological photonics, Nat. Photonics **8**, 821 (2014).
[4] T. Ozawa, H. M. Price, A. Amo, N. Goldman, M. Hafezi, L. Lu, M. C. Rechtsman, D. Schuster, J. Simon, O. Zilberberg, and I. Carusotto, Topological photonics, Rev. Mod. Phys. **91**, 015006 (2019).
[5] N. R. Cooper, J. Dalibard, and I. B. Spielman, Topological bands for ultracold atoms, Rev. Mod. Phys. **91**, 015005 (2019).
[6] G. Ma, M. Xiao, and C. T. Chan, Topological phases in acoustic and mechanical systems, Nat. Rev. Phys. **1**, 281 (2019).
[7] F. Wilczek and A. Zee, Linking Numbers, Spin, and Statistics of Solitons, Phys. Rev. Lett. **51**, 2250 (1983).
[8] J. E. Avron, R. Seiler, and B. Simon, Homotopy and Quantization in Condensed Matter Physics, Phys. Rev. Lett. **51**, 51 (1983).
[9] C.-K. Chiu, J. C. Y. Teo, A. P. Schnyder, and S. Ryu, Classification of topological quantum matter with symmetries, Rev. Mod. Phys. **88**, 035005 (2016).
[10] D. J. Thouless, M. Kohmoto, M. P. Nightingale, and M. denNijs, Quantized Hall Conductance in a Two-Dimensional Periodic Potential, Phys. Rev. Lett. **49**, 405 (1982).
[11] S.-C. Zhang and J. Hu, A four-dimensional generalization of the quantum Hall effect, Science **294**, 823 (2001).
[12] J. Zak, Berry's Phase for Energy Bands in Solids, Phys. Rev. Lett. **62**, 2747 (1989).
[13] R. D. King-Smith and D. Vanderbilt, Theory of polarization of crystalline solids, Phys. Rev. B **47**, 1651 (1993).
[14] R. Resta, Theory of the electric polarization in crystals, Ferroelectrics **136**, 51 (1992).
[15] R. Resta, Manifestations of Berry's phase in molecules and condensed matter, J. Phys. Condens. Matter **12**, R107 (2000).
[16] D. Xiao, M.-C. Chang, and Q. Niu, Berry phase effects on electronic properties, Rev. Mod. Phys. **82**, 1959 (2010).
[17] N. Marzari, A. A. Mostofi, J. R. Yates, I. Souza, and D. Vanderbilt, Maximally localized Wannier functions: Theory and applications, Rev. Mod. Phys. **84**, 1419 (2012).
[18] W. A. Benalcazar, B. A. Bernevig, and T. L. Hughes, Electric multipole moments, topological multipole moment pumping, and chiral hinge states in crystalline insulators, Phys. Rev. B **96**, 245115 (2017).
[19] W. A. Benalcazar, B. A. Bernevig, and T. L. Hughes, Quantized electric multipole insulators, Science **357**, 61 (2017).
[20] J. E. Moore, Y. Ran, and X.-G. Wen, Topological Surface States in Three-Dimensional Magnetic Insulators, Phys. Rev. Lett. **101**, 186805 (2008).
[21] A. M. Essin, J. E. Moore, and D. Vanderbilt, Magnetoelectric Polarizability and Axion Electrodynamics in Crystalline Insulators, Phys. Rev. Lett. **102**, 146805 (2009).
[22] M. Z. Hasan and J. E. Moore, Three-dimensional topological insulators, Annu. Rev. Condens. Matter Phys. **2**, 55 (2011).
[23] C. L. Kane and E. J. Mele, Quantum Spin Hall Effect in Graphene, Phys. Rev. Lett. **95**, 226801 (2005).
[24] C. L. Kane and E. J. Mele, Z_2 Topological Order and the Quantum Spin Hall Effect, Phys. Rev. Lett. **95**, 146802 (2005).
[25] B. A. Bernevig, T. L. Hughes, and S.-C. Zhang, Quantum spin Hall effect and topological phase transition in HgTe quantum wells, Science **314**, 1757 (2006).
[26] L. Fu, Topological Crystalline Insulators, Phys. Rev. Lett. **106**, 106802 (2011).
[27] L. Fu, C. L. Kane, and E. J. Mele, Topological Insulators in Three Dimensions, Phys. Rev. Lett. **98**, 106803 (2007).
[28] Y. Xia, D. Qian, D. Hsieh, L. Wray, A. Pal, H. Lin, A. Bansil, D. Grauer, Y. S. Hor, R. J. Cava, and M. Z. Hasan, Observation of a large-gap topological-insulator class with a single Dirac cone on the surface, Nat. Phys. **5**, 398 (2009).

[29] H. Zhang, C.-X. Liu, X.-L. Qi, X. Dai, Z. Fang, and S.-C. Zhang, Topological insulators in Bi_2Se_3, Bi_2Te_3 and Sb_2Te_3 with a single Dirac cone on the surface, Nat. Phys. **5**, 438 (2009).

[30] Z. Wang, X.-L. Qi, and S.-C. Zhang, Equivalent topological invariants of topological insulators, New J. Phys. **12**, 065007 (2010).

[31] F. Tang, Y. Ren, P. Wang, R. Zhong, J. Schneeloch, S. A. Yang, K. Yang, P. A. Lee, G. Gu, Z. Qiao, and L. Zhang, Three-dimensional quantum Hall effect and metal–insulator transition in $ZrTe_5$, Nature (London) **569**, 537 (2019).

[32] Y. Yang, Z. Gao, H. Xue, L. Zhang, M. He, Z. Yang, R. Singh, Y. Chong, B. Zhang, and H. Chen, Realization of a three-dimensional photonic topological insulator, Nature (London) **565**, 622 (2019).

[33] S. H. Kooi, G. van Miert, and C. Ortix, Hybrid-order topology of weak topological insulators, Phys. Rev. B **102**, 041122(R) (2020).

[34] L. Yuan, Q. Lin, M. Xiao, and S. Fan, Synthetic dimension in photonics, Optica **5**, 1396 (2018).

[35] M. Lohse, C. Schweizer, H. M. Price, O. Zilberberg, and I. Bloch, Exploring 4D quantum Hall physics with a 2D topological charge pump, Nature (London) **553**, 55 (2018).

[36] O. Zilberberg, S. Huang, J. Guglielmon, M. Wang, K. P. Chen, Y. E. Kraus, and M. C. Rechtsman, Photonic topological boundary pumping as a probe of 4D quantum Hall physics, Nature (London) **553**, 59 (2018).

[37] E. Lustig, S. Weimann, Y. Plotnik, Y. Lumer, M. A. Bandres, A. Szameit, and M. Segev, Photonic topological insulator in synthetic dimensions, Nature (London) **567**, 356 (2019).

[38] A. Dutt, Q. Lin, L. Yuan, M. Minkov, M. Xiao, and S. Fan, A single photonic cavity with two independent physical synthetic dimensions, Science **367**, 59 (2020).

[39] Z.-G. Chen, W. Zhu, Y. Tan, L. Wang, and G. Ma, Acoustic Realization of a Four-Dimensional Higher-Order Chern Insulator and Boundary-Modes Engineering, Phys. Rev. X **11**, 011016 (2021).

[40] X. Ni, K. Chen, M. Weiner, D. J. Apigo, C. Prodan, A. Alù, E. Prodan, and A. B. Khanikaev, Observation of Hofstadter butterfly and topological edge states in reconfigurable quasi-periodic acoustic crystals, Commun. Phys. **2**, 55 (2019).

[41] Q. Wang, M. Xiao, H. Liu, S. Zhu, and C. T. Chan, Optical Interface States Protected by Synthetic Weyl Points, Phys. Rev. X **7**, 031032 (2017).

[42] X. Fan, C. Qiu, Y. Shen, H. He, M. Xiao, M. Ke, and Z. Liu, Probing Weyl Physics with One-Dimensional Sonic Crystals, Phys. Rev. Lett. **122**, 136802 (2019).

[43] Y. Kim, C. L. Kane, E. J. Mele, and A. M. Rappe, Layered Topological Crystalline Insulators, Phys. Rev. Lett. **115**, 086802 (2015).

[44] Y. E. Kraus and O. Zilberberg, Topological Equivalence between the Fibonacci Quasicrystal and the Harper Model, Phys. Rev. Lett. **109**, 116404 (2012).

[45] P. G. Harper, The general motion of conduction electrons in a uniform magnetic field, with application to the diamagnetism of metals, Proc. Phys. Soc. London Sect. A **68**, 879 (1955).

[46] See Supplemental Material at http://link.aps.org/supplemental/10.1103/PhysRevLett.127.214302 for a 3D LCI sustaining only type-I TSMs, elastic implementation of the tight-binding model, elastic realization of 1D Harper chain and Su-Schrieffer-Heeger chain, and elastic realization of a 3D LCI sustaining only type-I TSMs, design of the elastic metacrystals, the effect of δl, and topological waveguiding in the synthetic 3D LCI.

[47] M. Miniaci, R. K. Pal, B. Morvan, and M. Ruzzene, Experimental Observation of Topologically Protected Helical Edge Modes in Patterned Elastic Plates, Phys. Rev. X **8**, 031074 (2018).

[48] K. H. Matlack, M. Serra-Garcia, A. Palermo, S. D. Huber, and C. Daraio, Designing perturbative metamaterials from discrete models, Nat. Mater. **17**, 323 (2018).

[49] M. Serra-Garcia, V. Peri, R. Süsstrunk, O. R. Bilal, T. Larsen, L. G. Villanueva, and S. D. Huber, Observation of a phononic quadrupole topological insulator, Nature (London) **555**, 342 (2018).

[50] M. Miniaci, R. K. Pal, R. Manna, and M. Ruzzene, Valley-based splitting of topologically protected helical waves in elastic plates, Phys. Rev. B **100**, 024304 (2019).

[51] Q. Wu, H. Chen, X. Li, and G. Huang, In-plane second-order topologically protected states in elastic kagome lattices, Phys. Rev. Applied **14**, 014084 (2020).

[52] S. H. Kooi, G. van Miert, and C. Ortix, Inversion-symmetry protected chiral hinge states in stacks of doped quantum Hall layers, Phys. Rev. B **98**, 245102 (2018).

[53] A. Dutt, M. Minkov, I. A. D. Williamson, and S. Fan, Higher-order topological insulators in synthetic dimensions, Light **9**, 131 (2020).

[54] X. Zhang, B.-Y. Xie, H.-F. Wang, X. Xu, Y. Tian, J.-H. Jiang, M.-H. Lu, and Y.-F. Chen, Dimensional hierarchy of higher-order topology in three-dimensional sonic crystals, Nat. Commun. **10**, 5331 (2019).

[55] C. He, H.-S. Lai, B. He, S.-Y. Yu, X. Xu, M.-H. Lu, and Y.-F. Chen, Acoustic analogues of three-dimensional topological insulators, Nat. Commun. **11**, 2318 (2020).

[56] H. Xue, Y. Ge, H.-X. Sun, Q. Wang, D. Jia, Y.-J. Guan, S.-Q. Yuan, Y. Chong, and B. Zhang, Observation of an acoustic octupole topological insulator, Nat. Commun. **11**, 2442 (2020).

[57] X. Ni, M. Li, M. Weiner, A. Alù, and A. B. Khanikaev, Demonstration of a quantized acoustic octupole topological insulator, Nat. Commun. **11**, 2108 (2020).

[58] Q. Wei, X. Zhang, W. Deng, J. Lu, X. Huang, M. Yan, G. Chen, Z. Liu, and S. Jia, Higher-order topological semimetal in acoustic crystals, Nat. Mater. **20**, 812 (2021).

[59] Z. Wang, Y. Chong, J. D. Joannopoulos, and M. Soljačić, Observation of unidirectional backscattering-immune topological electromagnetic states, Nature (London) **461**, 772 (2009).

[60] L. M. Nash, D. Kleckner, A. Read, V. Vitelli, A. M. Turner, and W. T. M. Irvine, Topological mechanics of gyroscopic metamaterials, Proc. Natl. Acad. Sci. U.S.A. **112**, 14495 (2015).

[61] Y. Ding, Y. Peng, Y. Zhu, X. Fan, J. Yang, B. Liang, X. Zhu, X. Wan, and J. Cheng, Experimental Demonstration of Acoustic Chern Insulators, Phys. Rev. Lett. **122**, 014302 (2019).

[62] F. Zangeneh-Nejad and R. Fleury, Topological Fano Resonances, Phys. Rev. Lett. **122**, 014301 (2019).
[63] F. Zangeneh-Nejad and R. Fleury, Topological analog signal processing, Nat. Commun. **10**, 2058 (2019).
[64] W. Wang, Y. Jin, W. Wang, B. Bonello, B. Djafari-Rouhani, and R. Fleury, Robust Fano resonance in a topological mechanical beam, Phys. Rev. B **101**, 024101 (2020).